

# Half-metallic and magnetic semiconducting behaviors of metal-doped blue phosphorus nanoribbon from first-principles calculations

Si-Cong Zhu,<sup>1), a, b</sup> Cho-Tung Yip,<sup>b, d</sup> Shun-Jin Peng,<sup>a</sup> Kai-Ming Wu,<sup>a</sup> Kai-Lun Yao,<sup>c</sup> Chee-Leung Mak<sup>b</sup> and Chi-Hang Lam<sup>2), b</sup>

a. College of Science and Key Laboratory for Ferrous Metallurgy and Resources Utilization of Ministry of Education, Wuhan University of Science and Technology, Wuhan 430065, China

b. Department of Applied Physics, Hong Kong Polytechnic University, Hung Hom, Hong Kong, China

c. Wuhan National High Magnetic Field Center and School of Physics, Huazhong University of Science and Technology, Wuhan 430074, China

d. Department of Physics, Shenzhen Graduate School, Harbin Institute of Technology, Shenzhen 518055, China

E-mail:<sup>1)</sup> [sczhu@wust.edu.cn](mailto:sczhu@wust.edu.cn), <sup>2)</sup> [C.H.Lam@polyu.edu.hk](mailto:C.H.Lam@polyu.edu.hk)

We investigate the electronic and magnetic properties of substitutional metal atom impurities in two-dimensional (2D) blue phosphorene nanoribbons using the first-principles calculations. In impure zigzag blue phosphorene nanoribbons (zBPNRs), a metal atom substitutes for a P atom at position “A/B”. The V-“B” structure shows half-metallic properties, while the Mn-“A/B”, V-“A”, Fe-“B”, and Cr-“A/B” structures show magnetic semiconductor properties. In addition, the Fe-“A” system shows magnetic metallic properties. On the other hand, for metal-doped armchair blue phosphorene nanoribbons (aBPNRs), the Mn-“A/B”, V-“A”, Fe-“A/B”, and Cr-“A/B” structures show magnetic semiconductor properties, while the V-“B” structure shows nonmagnetic properties. We find that the magnetic properties of such substitutional impurities can be understood regarding the exchange splitting of the metal 3d orbitals. And from analyzing the electron orbitals, the main contribution of the DOS for every system comes from the d and p orbitals. These results provide excellent candidates of new magnetic semiconductors and half-metals for spintronic devices based on blue phosphorenes.

## 1. Introduction

Two-dimensional (2D) materials, including graphene, molybdenum disulfide, silicene and black phosphorus, are currently the subject of intense theoretical and experimental research due to their potential for novel electronic device applications.<sup>1-5</sup> Significant efforts have been undertaken to understand its mechanical, electronic, thermal, magnetic, and other properties.<sup>6-12</sup> One most enticing applications is spintronic devices confined within the two dimensional (2D) materials. Graphene, due to the lack a natural band gap, is not readily

applicable. The electronic band gap is an intrinsic property of semiconductors that determines the electronic transport and governs the operation of electronic devices. For this, many other 2D materials are explored theoretically and experimentally.<sup>13-17</sup>

Very recently, a new 2D material, black phosphorene, has been successfully fabricated through exfoliation from bulk black phosphorus.<sup>18</sup> Black phosphorene presents some advantages superior to other previously studied 2D semiconductors because of its electronic properties, thereby drawing enormous interest in materials science.<sup>19-25</sup>

An allotrope of black phosphorene with a non-coplanar hexagonal structure of phosphorus is “blue phosphorus”. It can be transformed from black phosphorus by particular dislocations. Similar to silicene, blue phosphorus also has a buckled honeycomb structure. However, different to the zero band gap of graphene and the narrow band gap of around 0.5 eV of black phosphorus, blue phosphorus displays a wide fundamental band gap. In 2016,<sup>26</sup> Zhang has developed a molecular beam epitaxy (MBE) process for the epitaxial growth of uniform single layer blue phosphorus on Au (111) by using black phosphorus as a precursor. The realization of epitaxial growth of large-scale and high quality atomic-layered blue phosphorus can enable the rapid development of novel electronic and optoelectronic devices based on this emerging two-dimensional material.<sup>27</sup>

Indeed, the confinement of the electronic wave functions and the presence of the edges adjust the band gap, making 2D material suitable for the realization of devices. Due to their potential technological applications, their electronic structure has been widely investigated<sup>28</sup> with particular attention on the factors determining the presence of the gap. The electronic and magnetic properties of blue phosphorene have been intensively studied theoretically.<sup>29-32</sup> However, the magnetism of blue phosphorus nanoribbon remains a question. The most appealing and conventional technique to induce magnetic properties in a nonmagnetic material is magnetic transition metal impurity doping or creation of vacancy defects in the host material. In this work, we show that metal atom doped blue phosphorene nanoribbons (BPNRs) with hydrogen passivated armchair and zigzag shaped edges have both non-zero band gaps and spin polarizations.

Along specific directions, blue phosphorus can be tailored to zigzag-type blue phosphorene nanoribbons (zBPNRs) and armchair-type blue phosphorene nanoribbons (aBPNRs). When the edge P atoms are saturated by H atoms, zBPNRs and aBPNRs display nonmagnetic semiconducting behaviors, and their band gaps can be enhanced to be about 2.5eV.<sup>28</sup> In this paper, we aim to explore the magnetic properties of metal-doped blue phosphorene layer systems. Our study may provide useful information regarding the potential magnetic semiconductor applications. We will explore whether the phosphorene

layer can be utilized as a magnetic semiconductor system. Besides, the possibility of half-metallicity induced by metals impurities for spintronics will be studied as well. In this regard, we will consider substitution doping by a series of magnetic metal atoms such as V, Cr, Mn, Fe, and Ni, which may show spin polarization properties.

## 2. Computational method

We have performed all the calculations using the spin-polarized density functional theory (DFT) using Virtual NanoLab & Atomistix ToolKit (VNL-ATK).<sup>33-35</sup> DFT calculations based on the conventional Kohn–Sham Hamiltonian are performed using the local density approximation (LDA)-PZ (Perdew, Zunger). A double- $\zeta$  polarized basis set is used for expanding the electronic density.  $8 \times 4 \times 2$  K-points are sampled in the Brillouin zone (BZ) of the contact region. The density mesh cut-off is 150 Rydberg and the maximum force is  $0.05 \text{ eV } \text{\AA}^{-1}$  during geometry optimizations. We use different metal atoms to substitute for the phosphorus atoms in zigzag and armchair blue phosphorus nanoribbons. Generalized gradient approximation (GGA) - Perdew-Burke-Ernzerhof (PBE) is also used and it provides very similar results. The blue phosphorus nanoribbons (BPNRs) we studied are schematically shown in Figure 1, representing a pristine 6-zigzag BPNR and a 9-armchair BPNR. In order to avoid spurious interactions due to the periodic boundary conditions, vacuum region  $10 \text{\AA}$  thick along the Y and Z direction are introduced. BPNRs with hydrogen passivated armchair and zigzag edges have been investigated. The band gaps of undoped zigzag and armchair blue phosphorus nanoribbon are also shown in the figure 1. We substitute phosphorous atoms by magnetic metal atoms (V, Cr, Mn, Fe, and Ni) at position “A” or “B” as shown in Figure 1(a)-(b). It is worth noting that the super cell and the lattice are optimized to obtain the most stable atomic positions in each case.

## 3. Results and discussion

### (a) Zigzag blue phosphorus nanoribbon

The band structures of metal atoms doped zBPNRs are plotted in Figure 2. We observe energy level splitting between the majority spin and minority spin channels near the Fermi level, which induces magnetic moments. As indicated in the band structures, the band gaps are narrower than those of undoped blue phosphorus nanoribbons. As shown in Figure 2b for zBPNR V-doped at position “B”, the majority-spin conducting band shifts downward across the Fermi level and yields metallicity, while the minority-spin channel remains semiconducting with a gap of 1.01 eV. Therefore, the material becomes half-metallic. We

have also optimized the wider nanoribbons of V-“B”-doped zBPNR, the structure and the band structure show the similar properties of the narrow ones, zBPNR Fe-doped at position “A” shows a spin polarized metallic character as both the majority and minority spin bands cross the Fermi level (see Figure 2g). The Ni doped systems show nonmagnetic metallic character (see Figure 2i and 2j). For the other doped zBPNR structures, the spin channels for the majority and minority spins have different band gaps.

The partial density of states (PDOS) of metal atoms doped zBPNR is shown in Figure 3. The PDOS of the majority and minority states are completely compensated with each other, yielding zero spin moment in Ni-“A” and Ni-“B”-doped systems (see Figure 3). In the other systems, we find that the major source of spin polarization of each metal atom originated from different electron orbitals. For instance, the V-“B” doping impurity states imply that the half-metallic behavior is mainly contributed from the V 3d orbitals as shown in figure 3. In the case of Fe-“A” doping impurity states (see Figure 3), the bottom of the conduction band and the top of the valence band are dominated by P 2p states of the majority spin channel, while the minority spin states are mainly dominated by the Fe 3d states. The main contributing electron orbitals of the majority and minority spins, the magnetic moment and the binding energy for all the impurity structures are displayed in Table 1. The V-“A” doped zBPNR leads to the most stable impurity states due to its maximum binding energy. We have also performed GGA+U calculations to our blue phosphorus nanoribbon. A single U parameter is used, which we have taken as an empirical parameter varied in the range 2.5eV for all the studied impurities. Most results are quantitatively similar. Only for V-“B” doped zBPNR, GGA+U results shows significant (qualitative) differences with respect to the results of PBE-GGA calculations with no band crossing the Fermi level. The half metallic character thus disappears and the V-“B” doped zBPNR only behaves as a magnetic semiconductor (see Figure S1).

To further verify the reason of the half-metallic (HM) and metallic behaviors, we analyze the spin density and electronic orbital states and results are shown in Table 2. For the V-“B”-doped system, the majority spin density is much larger than the minority spin density. Also, the spin density is localized at the V atom and edge P atoms. The major contribution to the magnetic moment stems from the  $d_{xy}$  orbital for the LUMO of the majority spin channel. For the HOMO of the minority spin channel, the V loses all the electrons and this shows that non 3d electron states cause the HM character. In the Fe-“A” doped system, the majority spin density is similar to the minority spin density which indicates small polarizability. The  $p_z$ ,  $p_x$ ,  $d_{yz}$ ,  $d_{xy}$  orbitals are the major source of spin polarization in the majority spin channel. The electrons in Fe 3d and the near P 2p states

are delocalized and distributed around both the P atoms and their bonds. Therefore, it greatly enhances the conductivity, causing the metallic property. In minority spin channel, the  $d_{z^2}$  electrons give rise to the negative magnetic moment of the Fe atom. These results agree with the calculated band structure and the spin densities.

#### **(b). Armchair blue phosphorus nanoribbon**

The band structures of metal atoms doped aBPNR are plotted in Figure 4. All the structures are semiconductors. Only the V-“B” doped system shows a zero spin magnetic moment as indicated in table 1 and this leads to a zero spin polarization as observed in Figure 4b. The Ni-doped system shows a spin polarization (see Figure 4i and 4j)), in contrast to the different property of zBPNR.

In Figure 5, we present the partial density of states (PDOS) of metal atoms doped aBPNR. All structures have Fermi levels in between the band gaps showing semiconducting characteristics. Only for V-“B” doped blue phosphorenes, the PDOS of the majority and minority states are completely compensated with each other, yielding a zero spin magnetic moment (see Figure 5). The PDOS of the majority spin for the V-“A” doped structure shows a smaller band gap than that of the minority spins (see Figure 5) resulting at a spin polarization. Fe-, Mn-, Ni- and Cr-doped aBPNRs show magnetic semiconductor characters (see Figure 5).

The electronic orbital states of V-“A” and V-“B” doped aBPNR are listed in Table 3. For the spin polarized V-“A” doped aBPNR, we observe that the major source of spin polarization of V atom originates from the d-orbitals. For instance, the major contribution to the magnetic moment stems from the  $d_{xz}$  and  $d_{z^2}$  orbitals of the LUMO and HOMO while the  $p_z$  orbital is the major source of minority spin state. The PDOS of V-“A” doped aBPNR also shows the magnetic source of different electronic orbitals in figure 5. In the V-“B” doped system, electrons in V and the nearest P atoms have a strong orbital hybridization. The p and d orbitals show almost equal contributions to the PDOS.

#### **(c) Zigzag and armchair blue phosphorus nanoribbon**

The spin moments of substitution metals in BPNRs are displayed in Figure 6, together with those of the isolated metal atoms. The spin moments of the isolated metal atoms are  $2\mu_B$  (V),  $3\mu_B$  (Cr),  $4\mu_B$  (Mn),  $5\mu_B$  (Fe), and  $6\mu_B$  (Ni). The Ni-“A”, Ni-“B” zBPMR and V-“A” aBPMR have a zero magnetic moment, but it is  $3\mu_B$  for all the Cr doped systems. And the metal atoms lose electrons while the nearest phosphorous atoms gain electrons. The spin configurations of each doped systems are shown in Table 4. The spin alignment results are

consistent with Hund's-rule, and therefore paired electrons and itinerant electrons occupy different d states, as was originally suggested by Goodenough.<sup>36</sup> We note that the valence electron configurations of V, Cr, Mn, Fe, and Ni are  $3d^34s^2$ ,  $3d^54s^1$ ,  $3d^54s^2$ ,  $3d^64s^2$ , and  $3d^84s^2$ , respectively.

In brief, we can identify several regimes depending on the filling of the electronic levels: For zBPNR:(i) Ni-“A” and Ni-“B” doped zBPNRs have fully occupied Ni-phosphorous bonding levels, leading to a zero spin moment and the low spin states of Ni+2.(ii) Mn-“B”, Fe-“A”, and Fe-“B” doped zBPNRs have partially occupied metal-phosphorous bonding levels with spin moments of 2.00, 2.00, and 3.00  $\mu_B$ , respectively.(iii) Mn-“A”, V-“A/B” and Cr-“A/B” doped zBPNRs have partially occupied non-bonding 3d levels with spin moments of 4.00, 2.00, and 3.00 $\mu_B$  respectively. In (ii) and (iii), Mn-“A” and Mn-“B” each lose 3 electrons, and the “A” position exhibits a high spin state, but “B” position shows a low spin state.

For aBPNR:(i) V-“B” doped BPNR has empty V-phosphorous bonding levels, because the V atom loses 5 electrons, which leads to a zero spin moment of V-“B” doped system. (ii) Fe-“A”, Fe-“B”, and Ni-“A/B” structures have partially occupied metal-phosphorous bonding levels with spin moments of 3.00, 1.00, 1.00, and 1.00  $\mu_B$ , respectively.(iii) Mn-, V-“A” and Cr-“A/B” structures have partially occupied non-bonding 3d levels with spin moments of 4.00, 2.00 and 3.00 $\mu_B$ .

#### (d) Spin transport

For the V-“B” zBPNR device applications, a more direct and reliable approach to determine its half metal nature is the ab initio quantum transport simulation. To calculate spin-dependent transport properties, we also make use of the first principles quantum transport package VNL-ATK where DFT is carried out with in the Keldysh nonequilibrium Green's function formalism. The basic principle and practical implementation of the NEGF-DFT formalism can be found in Ref. [37]. Essentially, within NEGF-DFT the device Hamiltonian and electronic structure are determined by DFT, the nonequilibrium quantum statistics of the device physics is determined by NEGF, and the transport boundary conditions under external bias are handled by real space numerical techniques. The NEGF-DFT self-consistency is controlled by a numerical tolerance of  $10^{-4}$ eV. Optimized basis sets of the double- $\xi$  quality including polarization functions are used with the real-space mesh cut-off 150 Ry. For infinite 2D nanoribbon, the Monkhorst-Pack  $1 \times 1 \times 100$  k-point grid is used to sample the 2D Brillouin zone. The spin-dependent transmission coefficients for spin channel  $\sigma_{\text{majority}}$  and  $\sigma_{\text{minority}}$  at energy E and bias voltage  $V_b$

are calculated as

$$T_{\sigma}(E, V_b) = \sum_{k_x k_y} \text{Tr}[\text{Im} \Sigma_L^r G^r \text{Im} \Sigma_R^r G^a] \quad (1)$$

And

$$T_{\sigma}(E, V_b) = \text{Tr}[T_{\sigma}(E, V_b)] \quad (2)$$

where the trace is over the basis functions. Here  $G^r$  is  $2n \times 2n$  NEGF matrix where 2 is due to spin and  $n$  is the size of the basis set;  $\Sigma^r$  is the self-energy describing the coupling between the semi-infinite ferromagnetic leads and the scattering region which includes pristine zBPNR segment and two parts of V-doped zBPNR leads. For our system,  $\Sigma_L^r$  is diagonal and given by

$$\sum_L^r(E) = \begin{pmatrix} \Sigma_{L_{\text{Maj.}}}^r(E) & 0 \\ 0 & \Sigma_{L_{\text{min.}}}^r(E) \end{pmatrix} \quad (3)$$

For parallel configuration,  $\Sigma_R^r$  is the same as  $\Sigma_L^r$  except changing subscript L to R. For parallel configuration,  $\Sigma_R^r$  is expressed as

$$\sum_R^r(E) = \begin{pmatrix} \Sigma_{R_{\text{maj.}}}^r(E) & 0 \\ 0 & \Sigma_{R_{\text{min.}}}^r(E) \end{pmatrix} \quad (4)$$

As an example, in Figure 7c, we present the simulated transport properties of the pristine 6-zigzag BPNR connected with V doped 6-zigzag BPNR electrodes. The spin-orbit coupling (SOC) is not included in the calculation. From the transmission coefficient shown in Figure 7c, we can see a 0.88eV transport gap of the minority spin channel while the majority electrons through the zBPNR show several transmission peaks located within  $-0.5$  and  $0.5$  eV (see inset of Figure 7c). We show the electron densities of the majority and minority spins for the sandwich system at 0V in Fig. 7(a) and 7(b), respectively. The majority spin density of the V atoms is larger than that of the minority one. This can provide a larger majority current to achieve towards a 100% spin filter effect (SEF defined as:  $SFE = [T(E_f)_{\text{Maj}} - T(E_f)_{\text{Min}}] / T(E_f)_{\text{Maj}} \times 100\% = 100\%$ , for  $T(E_f)_{\text{Min}} = 0$ ).

## 4. Summary

In summary, we have investigated magnetism in metal-doped BPNRs. Spin polarized states are observed in doped zBPNRs and aBPNRs. For zBPNRs it is found that when V atoms substitute P atoms at the “B” positions, half-metallic features of the ground state are observed. The Mn-“A/B”, V-“A”, Fe-“B”, and Cr-“A/B” structures exhibit magnetic semiconductor properties, while the Ni-“A/B” structures show nonmagnetic metallic

properties. In addition, the Fe-“A” system shows magnetic metallic properties. For aBPNR, the Mn-“A/B”, V-“A”, Fe-“A/B”, and Cr-“A/B” structures show magnetic semiconductor properties, while the V-“B” structure shows nonmagnetic properties. The presence of itinerant electron and dangling bond are crucial to the magnetic properties. The dangling bond states localized at the edges and the metal atoms contribute significantly to the total magnetic moment. Hydrogenated BPNRs are in contrast nonmagnetic since the dangling bonds are saturated. However, the doped BPNRs are spin polarized due to the weak P-M bond in the ribbon plane between the d-orbitals and the p-orbitals of the metal atoms and the P atoms respectively. We predict that the pristine 6-zigzag BPNR coupled to V doped 6-zigzag BPNR electrodes exhibits a near-perfect spin-filter effect.

## Acknowledgements

The authors would like to acknowledge the support from Hong Kong Scholars Program No. XJ2016007, National Natural Science Foundation of China under Grants No. 11647047, 11504078 and No. 11704291, and HK PolyU under Grant No. 1-ZVGH.

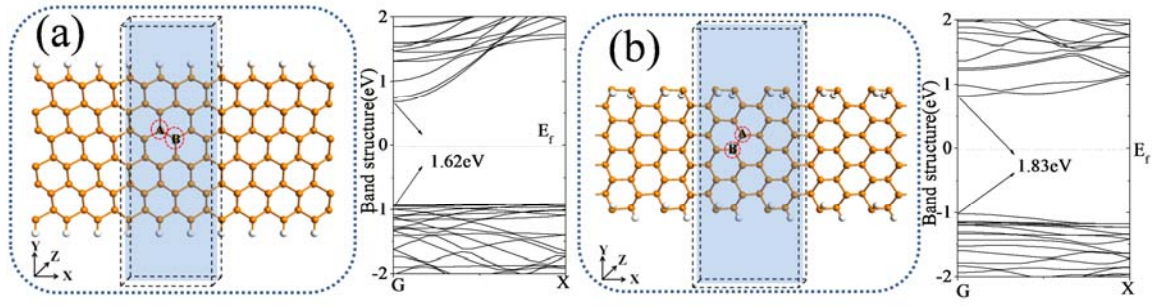
## References

1. A. Geim and I. Grigorieva, *Nature*, 2013, **499**, 419.
2. P. Vogt, P. De Padova, C. Quaresima, J. Avila, E. Frantzeskakis, M. C. Asensio, A. Resta, B. Ealet and G. Le Lay, *Physical review letters*, 2012, **108**, 155501.
3. L. Li, Y. Yu, G. J. Ye, Q. Ge, X. Ou, H. Wu, D. Feng, X. H. Chen and Y. Zhang, *Nature nanotechnology*, 2014, **9**, 372-377.
4. H. Liu, A. T. Neal, Z. Zhu, Z. Luo, X. Xu, D. Tománek and D. Y. Peide, 2014.
5. W. Lu, H. Nan, J. Hong, Y. Chen, C. Zhu, Z. Liang, X. Ma, Z. Ni, C. Jin and Z. Zhang, *Nano Research*, 2014, **7**, 853-859.
6. Y. Zhang, Y.-w. Tan, H. L. Stormer and P. Kim, *Nature*, 2005, **438**, 201-204.
7. A. C. Neto, F. Guinea, N. M. Peres, K. S. Novoselov and A. K. Geim, *Reviews of modern physics*, 2009, **81**, 109.
8. M. A. Rafiee, Rensselaer Polytechnic Institute, 2011.
9. R. R. Nair, P. Blake, A. N. Grigorenko, K. S. Novoselov, T. J. Booth, T. Stauber, N. M. Peres and A. K. Geim, *Science*, 2008, **320**, 1308-1308.
10. A. C. Ferrari, J. Meyer, V. Scardaci, C. Casiraghi, M. Lazzeri, F. Mauri, S. Piscanec, D. Jiang, K. Novoselov and S. Roth, *Physical review letters*, 2006, **97**, 187401.
11. A. K. Geim and K. S. Novoselov, *Nature materials*, 2007, **6**, 183-191.
12. P. R. Wallace, *Physical Review*, 1947, **71**, 622.



13. M. Corso, W. Auwärter, M. Muntwiler, A. Tamai, T. Greber and J. Osterwalder, *Science*, 2004, **303**, 217-220.
14. M. Si, D. Gao, D. Yang, Y. Peng, Z. Zhang, D. Xue, Y. Liu, X. Deng and G. Zhang, *The Journal of chemical physics*, 2014, **140**, 204701.
15. X. Niu, X. Mao, D. Yang, Z. Zhang, M. Si and D. Xue, *Nanoscale research letters*, 2013, **8**, 469.
16. Z. Zhang, M. Si, Y. Wang, X. Gao, D. Sung, S. Hong and J. He, *The Journal of chemical physics*, 2014, **140**, 174707.
17. S. Lebègue, T. Björkman, M. Klintonberg, R. M. Nieminen and O. Eriksson, *Physical Review X*, 2013, **3**, 031002.
18. E. S. Reich, *Nature*, 2014, **506**, 19.
19. Z. Zhu, C. Li, W. Yu, D. Chang, Q. Sun and Y. Jia, *Applied Physics Letters*, 2014, **105**, 113105.
20. V. Tran, R. Soklaski, Y. Liang and L. Yang, *Physical Review B*, 2014, **89**, 235319.
21. R. Fei and L. Yang, *Nano letters*, 2014, **14**, 2884-2889.
22. R. Fei and L. Yang, *Applied Physics Letters*, 2014, **105**, 083120.
23. V. Tran and L. Yang, *Physical Review B*, 2014, **89**, 245407.
24. Z.-L. Zhu, W.-Y. Yu, X.-Y. Ren, Q. Sun and Y. Jia, *EPL (Europhysics Letters)*, 2015, **109**, 47003.
25. W. Yu, Z. Zhu, C.-Y. Niu, C. Li, J.-H. Cho and Y. Jia, *Physical Chemistry Chemical Physics*, 2015, **17**, 16351-16358.
26. Z. Zhu and D. Tománek, *Physical review letters*, 2014, **112**, 176802.
27. J. L. Zhang, S. Zhao, C. Han, Z. Wang, S. Zhong, S. Sun, R. Guo, X. Zhou, C. D. Gu and K. D. Yuan, *Nano letters*, 2016, **16**, 4903-4908.
28. J. Xie, M. Si, D. Yang, Z. Zhang and D. Xue, *Journal of Applied Physics*, 2014, **116**, 073704.
29. A. Hashmi and J. Hong, *The Journal of Physical Chemistry C*, 2015, **119**, 9198-9204.
30. Y. Liu, X. Zhang, X. Yang, X. Hong, J. Feng, M. Si and X. Wang, *Physical Chemistry Chemical Physics*, 2015, **17**, 10462-10467.
31. Y. Du, H. Liu, B. Xu, L. Sheng, J. Yin, C.-G. Duan and X. Wan, *Scientific reports*, 2015, **5**.
32. W. Yu, Z. Zhu, C.-Y. Niu, C. Li, J.-H. Cho and Y. Jia, *Nanoscale research letters*, 2016, **11**, 77.
33. M. Khazaei, S. U. Lee, F. Pichierri and Y. Kawazoe, *ACS nano*, 2008, **2**, 939-943.
34. Z. Wang, T. Kadohira, T. Tada and S. Watanabe, *Nano letters*, 2007, **7**, 2688-2692.
35. M.-F. Ng, L. Shen, L. Zhou, S.-W. Yang and V. B. Tan, *Nano letters*, 2008, **8**, 3662-3667.
36. J. B. Goodenough, *Journal of Solid State Chemistry*, 1971, **3**, 490-500.
37. J. Taylor, H. Guo and J. Wang, *Physical Review B*, 2001, **63**, 245407.

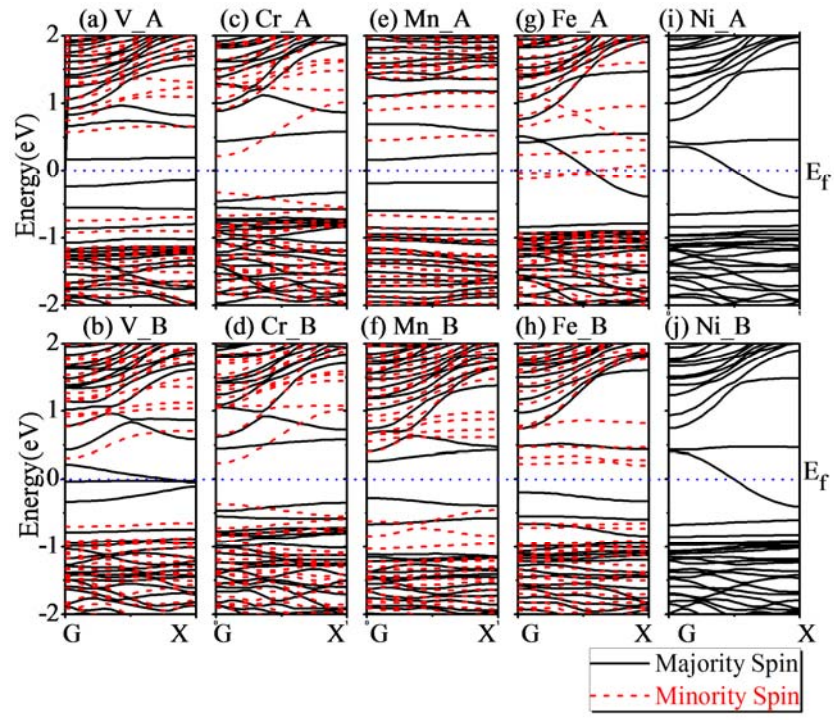
**Figure 1**



**FIG. 1.** Structures and band structures of (a) 6-zigzag BPNR and (b) 9-armchair BPNR. X is the cutting direction. The labels “A” and “B”

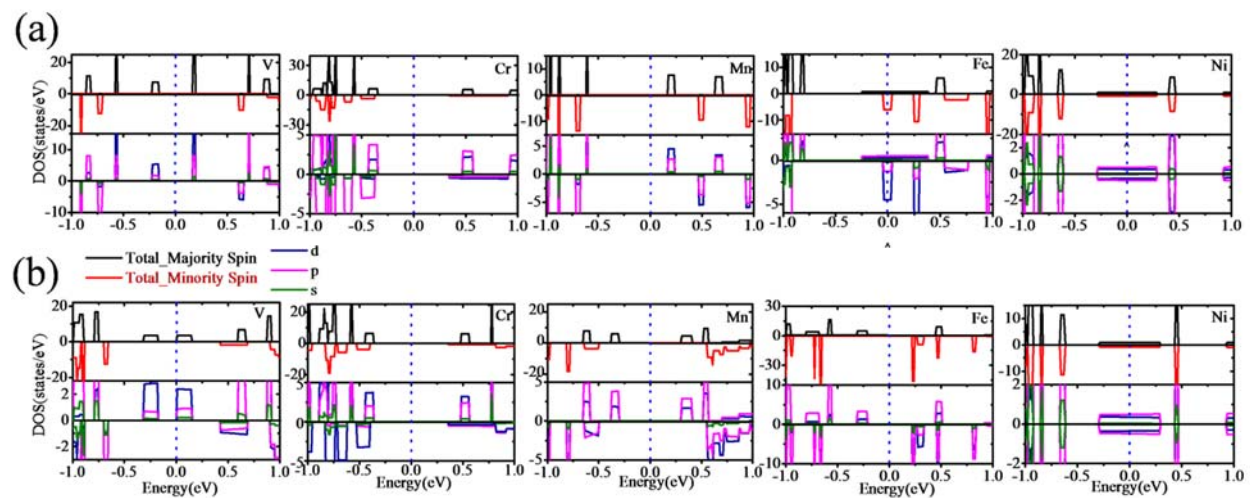
denote the substitutional sites. Hydrogen: hoar; Phosphorus: orange.

**Figure 2**



**FIG. 2.** Band structures of zBPNRs doped at position “A” and “B”.

**Figure 3**


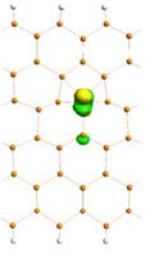
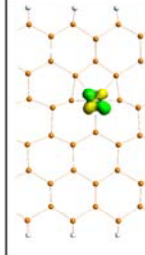
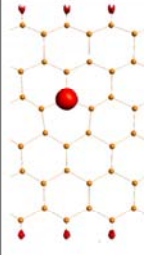
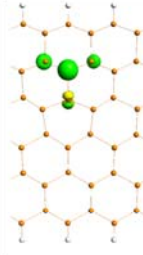
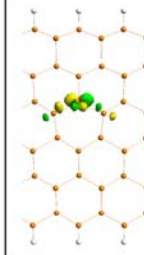

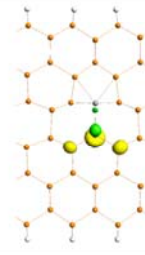
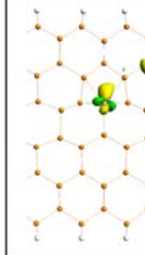
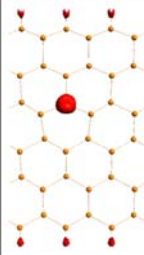
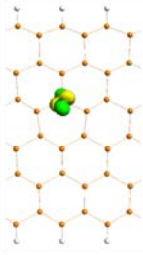
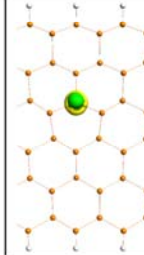


**FIG. 3.** Spin polarized partial density of states of zigzag-blue phosphorenes nanoribbons doped at position “A” (a) and “B” (b). The energy zero represents the Fermi level.

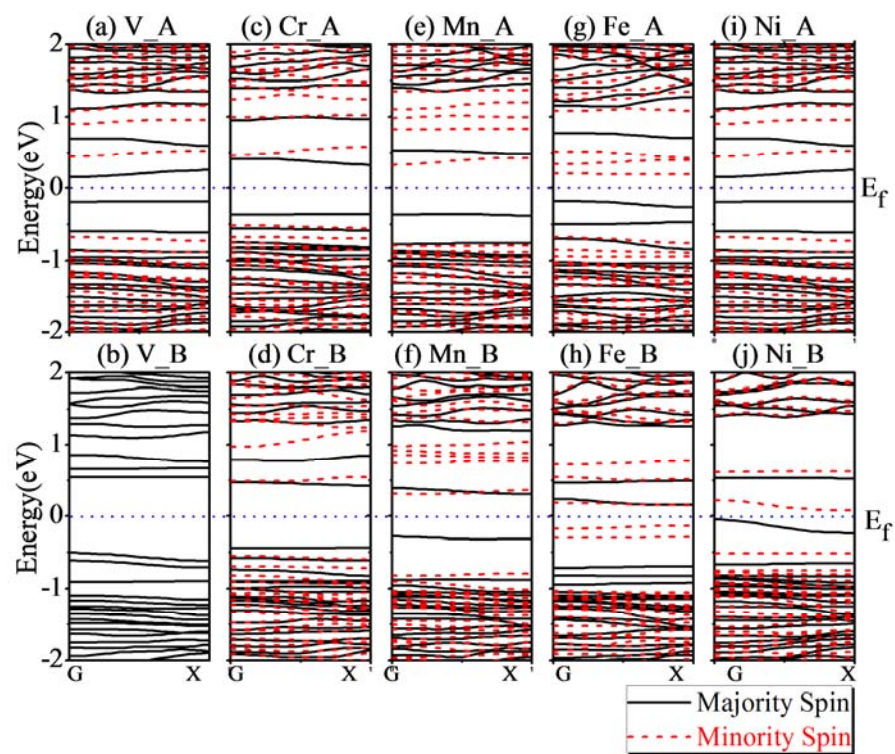
**Table1.** The main contributing electron orbitals of majority and minority spins, the magnetic moment, and the binding energy ( $E_b$ ) for the all impurity structures.

Metal Position		V			Cr			Mn			Fe			Ni		
Zigzag		Polarized		$\mu_B$	Polarized		$\mu_B$	Polarized		$\mu_B$	Polarized		$\mu_B$	Polarized		$\mu_B$
A	Majority	$\sqrt{\phantom{x}}$	p	2	$\sqrt{\phantom{x}}$	p	3	$\sqrt{\phantom{x}}$	d	4	$\sqrt{\phantom{x}}$	p	2	$\times$	d	0
	Minority		d			p			d							
	Eb(eV)		51.8		12.5		10.8		12.1		13.4					
B	Majority	$\sqrt{\phantom{x}}$ HM	p	2	$\sqrt{\phantom{x}}$	p	3	$\sqrt{\phantom{x}}$	p	2	$\sqrt{\phantom{x}}$	d	3	$\times$	d	0
	Minority		p			d			d							
	Eb(eV)		13.0		12.4		23.5		12.5		13.4					
Armchair																
A	Majority	$\sqrt{\phantom{x}}$	d	2	$\sqrt{\phantom{x}}$	p	3	$\sqrt{\phantom{x}}$	p	4	$\sqrt{\phantom{x}}$	p	3	$\sqrt{\phantom{x}}$	d	1
	Minority		d			p			d							
	Eb(eV)		48.6		8.2		44.5		8.6		40.1					
B	Majority	$\times$	d	0	$\sqrt{\phantom{x}}$	p	3	$\sqrt{\phantom{x}}$	p	4	$\sqrt{\phantom{x}}$	p	1	$\sqrt{\phantom{x}}$	p	1
	Minority		p			d			p&d							
	Eb(eV)		9.9		8.4		7.0		8.0		9.3					

**Table 2.** Spin density (with the isosurface of  $0.5 \text{ \AA}^{-3}$ ) and electron orbitals (with the isosurface of amplitude  $0.2 \text{ \AA}^{-3/2}$ ) states of HOMO, LUMO in systems: V-“B” and Fe-“A” doping zBPNR. Hydrogen: hoar; phosphorus: orange.

Zigzag	Blue Phosphorus doped by V at “B”			Blue Phosphorus doped by Fe at “A”		
	Spin Density	HOMO	LUMO	Spin Density	HOMO	LUMO
		$d_{z^2}$ & $p_z$	$d_{xy}$		$p_z$ & $d_{yz}$	$d_{xy}$ & $p_x$
Majority Spin						
Minority Spin		$p_z$ 	$d_{x^2-y^2}$ 		$d_{yz}$ 	$d_{z^2}$ 

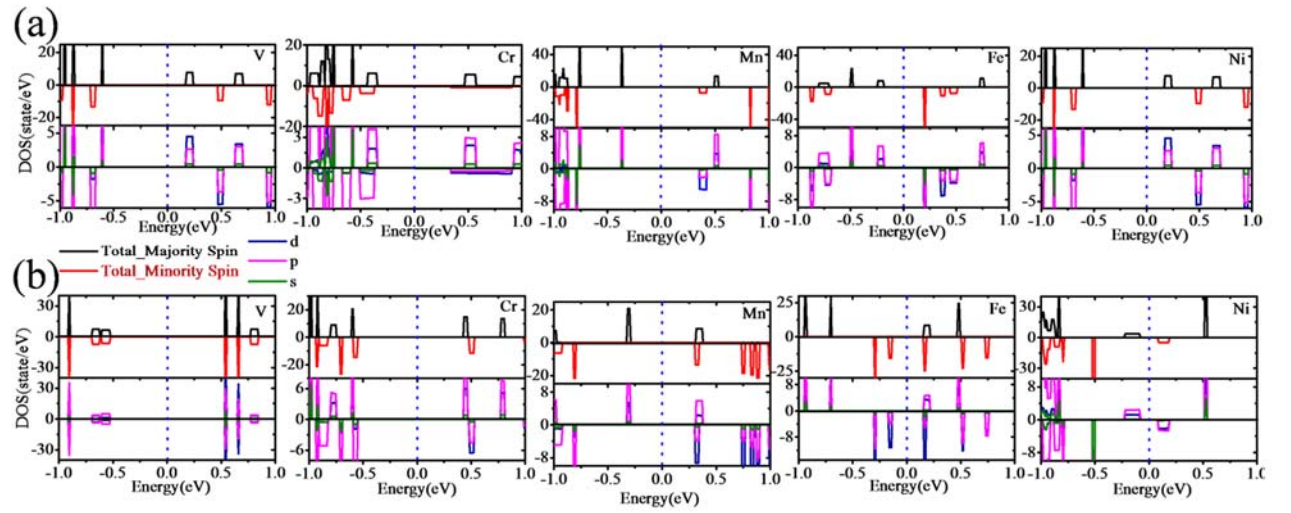
**Figure 4**



**FIG. 4.** Band structures of aBPNRs doped at position "A" and "B".



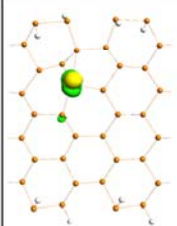
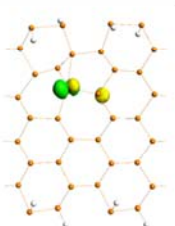
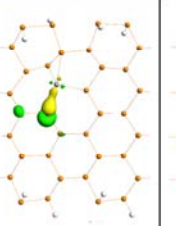
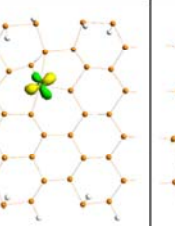
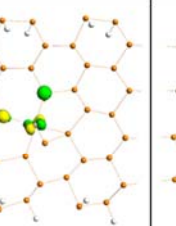
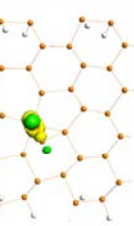
**Figure 5**



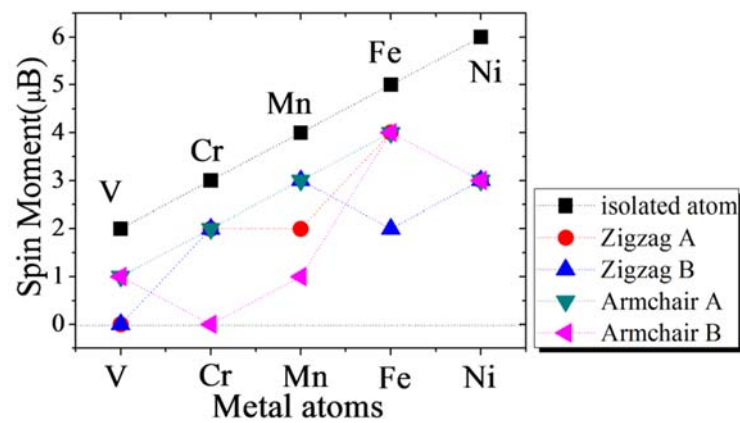
**FIG. 5.** Spin polarized partial density of states of armchair-blue phosphorenes nanoribbons doped at position "A" (a) and "B" (b). The energy zero represents the Fermi level.



**Table 3.** Electron orbitals states of HOMO and LUMO in V-“A” and V-“B” doped aBPNR with the isosurface of amplitude  $0.2 \text{ \AA}^{-3/2}$ . Hydrogen: hoar; phosphorus: orange.

Armchair					
doped by V at “A”				doped by V at “B”	
Majority Spin		Minority Spin			
HOMO	LUMO	HOMO	LUMO	HOMO	LUMO
$d_{z^2}$	$d_{xz}$	$P_z$	$d_{xy}$	$d_{xz}\&P_z$	$d_{z^2}\&P_z$
					

**Figure 6**

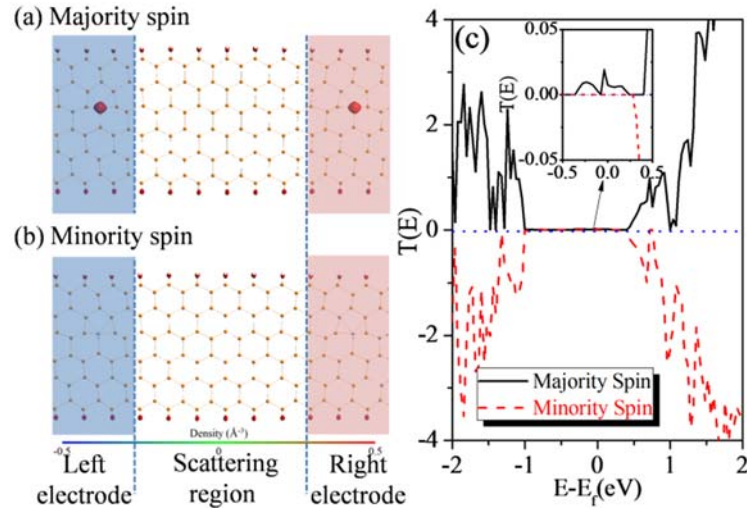


**FIG. 6.** Spin moments of the isolated metals and their substitutions in zBPNRs and zBPNRs as a function of the number of valence electrons.

**Table 4.** Hund's rule dependent spins electron arrangement in doped zBPNRs and aBPNRs.

Metal atoms	V	Cr	Mn	Fe	Ni
Orbital	$3d^34s^2$	$3d^54s^1$	$3d^54s^2$	$3d^64s^2$	$3d^84s^2$
Original spin	$\uparrow\uparrow\uparrow\downarrow$	$\uparrow\uparrow\uparrow\uparrow\uparrow$	$\uparrow\uparrow\uparrow\uparrow\uparrow\downarrow$	$\uparrow\downarrow\uparrow\uparrow\uparrow\uparrow\downarrow$	$\uparrow\downarrow\uparrow\downarrow\uparrow\downarrow\uparrow\uparrow\downarrow$
Zigzag A	$\uparrow\uparrow$	$\uparrow\uparrow\uparrow$	$\uparrow\uparrow\uparrow\uparrow$	$\uparrow\downarrow\uparrow\uparrow$	$\uparrow\downarrow\uparrow\downarrow\uparrow\downarrow$
Zigzag B	$\uparrow\uparrow$	$\uparrow\uparrow\uparrow$	$\uparrow\uparrow$	$\uparrow\downarrow\uparrow\uparrow\uparrow$	$\uparrow\downarrow\uparrow\downarrow\uparrow\downarrow$
Armchair A	$\uparrow\uparrow$	$\uparrow\uparrow\uparrow$	$\uparrow\uparrow\uparrow\uparrow$	$\uparrow\downarrow\uparrow\uparrow\uparrow$	$\uparrow\downarrow\uparrow\downarrow\uparrow\downarrow\uparrow$
Armchair B	None 3d	$\uparrow\uparrow\uparrow$	$\uparrow\uparrow\uparrow\uparrow$	$\uparrow\downarrow\uparrow$	$\uparrow\downarrow\uparrow\downarrow\uparrow\downarrow\uparrow$

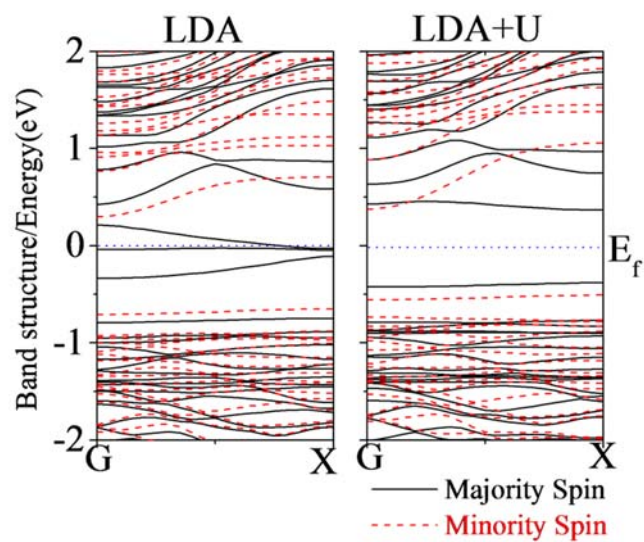
**Figure 7**



**FIG. 7.** Schematic diagram of a 6-zBPNR device where a pristine 6-zigzag BPNR is connected with the left- and right-hand BPNR leads. The BPNR leads are themselves 6-zigzag BPNRs but they are doped with Vanadium atoms. Device electron spin density of the majority spin (a) and the minority spin (b) with the isosurface of  $0.5 \text{ \AA}^{-3}$ . (c) The transmission coefficient of V-doped 6-zigzag BPNR device as a function of energy (Bias=0V). Inset: the spin transmission coefficient is within the energy window from  $-0.5$  to  $0.5$  eV at the bias 0V. Hydrogen: hoar; phosphorus: orange.

## Support information

Figure S1



**FIG. S1** The band structure of V-“B” doping zBPNR by LDA and LDA+U method